

ARTICLE OPEN



Stratospheric influences on surface ozone increase during the COVID-19 lockdown over northern China

Zhixiong Chen¹, Jane Liu^{1,2}✉, Xugeng Cheng¹, Mengmiao Yang¹ and Lei Shu¹

Surface ozone increased unexpectedly over northern China during the COVID-19 lockdown (CLD) period (23 January–29 February 2020), which was characterized by vigorous emission reduction. The reasons for this ozone enhancement have been speculated from perspectives of chemical responses to the emissions and meteorology. As known, the processes of natural stratospheric ozone injecting to the troposphere are most active in winter and spring. Yet, little attention was paid to stratospheric influences on this ozone enhancement. Here we report a stratospheric intrusion (SI) that reached the surface over northern China on 15–17 February during the CLD. The coevolution of enhanced ozone and sharply declined carbon monoxide and relative humidity (RH) was indicative of the SI occurrence. We show that the SI was facilitated by a cutoff low system that led to abnormally high surface ozone in most part of northern China. We estimate that over the SI period, the injected stratospheric ozone constituted up to 40–45% of the surface ozone over northern China. If the stratospheric ozone inputs were scaled over the entire CLD period, these inputs would account for 4–8% of the surface ozone. In view of the unexpected ozone increase during the CLD, this SI event could explain up to 18% of the ozone increase in some cities, and average 5–10% over larger areas that were affected. Hence, the nonnegligible stratospheric influences urge extra consideration of natural ozone sources in disentangling the role of emission reduction and meteorological conditions during the CLD in China and elsewhere in the world.

npj Climate and Atmospheric Science (2023)6:76; <https://doi.org/10.1038/s41612-023-00406-2>

INTRODUCTION

The Coronavirus Disease 2019 (COVID-19) outbreak in January 2020 provided a natural experiment to examine the roles of emission reduction and meteorology in surface ozone (O_3) variations. To prevent the spread of the COVID-19 epidemic, China adopted strict control measures including suspending industrial activity, restricting traffic transport, and releasing stay-at-home requirements (referred to as "lockdown"). As a result, it is found that primary air pollutants, such as nitrogen oxides ($NO_x = NO + NO_2$), sulfur dioxide (SO_2), carbon monoxide (CO), and volatile organic compound (VOC) declined sharply^{1–4}, however, surface ozone unexpectedly increased in China^{1–7}.

It is known that ozone concentrations vary with environmental factors such as precursor levels (including NO_x and VOCs) and meteorology. These factors, which integrally determine the photochemical production of ozone, have been investigated extensively to explain the unexpected ozone increase observed during the COVID-19 lockdown (CLD, 23 January–29 February 2020) period^{1–10}. Combining comprehensive observations and models, researchers have attributed the ozone increase to the nonlinearity of ozone chemical reactions, in which ozone increases when NO_x is significantly reduced, since China is generally characterized by a VOC-limited chemical regime in winter^{10–13}. The sharp NO_x reduction also strongly alleviated the nighttime titration of ozone and hence led to higher ozone concentrations. Impacts of meteorological conditions on the enhanced ozone during the CLD were also examined^{1,7,8}. Previous studies suggested that relative humidity (RH) increased considerably over northern China during the CLD, accompanied by lower wind speed and shallower planetary boundary layer height. Together with the seasonal cycle of meteorology, these meteorological conditions favored the formation and accumulation of ozone. In

addition, researchers disentangled the contributions of vigorous emission reduction and meteorological conditions to the unexpected ozone increase during the CLD by means of chemical transport models and machine learning technique^{1,14–16}.

Apart from the photochemically produced ozone, the downward transport of stratospheric ozone into the troposphere is a natural source of tropospheric ozone^{17–20}. Such stratospheric intrusion (SI) processes exhibit a pronounced seasonal variation with most activities in late winter and spring^{17,21,22}, and sometimes can transport substantial ozone to the surface^{23,24}. The vertically injected stratospheric ozone additively enhances the surface ozone concentrations and hence alters the normal diurnal cycle of ozone^{23–27}. While the stratosphere-to-troposphere (STT) exchange processes are irregular and uncontrollable, little attention has been paid to the potential stratospheric contributions to the ozone increase during the lockdown in coincidence with late winter season exhibiting high frequencies of SIs. Given the characteristics of stratospheric air mass (i.e., high ozone, low CO)¹⁷, the impacts of SIs can be mistakenly classified as the consequences of emission reduction, since the SI processes were not well resolved or considered in previous studies. As a result, the estimation of the impacts of emission reduction and meteorology would be biasedly blurred by possible SI events. Here, combining analysis of multisource observations, meteorological reanalysis data, and trajectory modeling, we report a deep SI event occurred over northern China and then assess its contributions to the surface ozone increase during the CLD. Using this deep SI case, we elucidate the nonnegligible influences of stratosphere on the surface ozone when disentangling the role of emission reduction and meteorological conditions. We believe these quantitative analyses of stratospheric ozone contributions would provide new

¹Key Laboratory for Humid Subtropical Eco-Geographical Processes of the Ministry of Education, School of Geographical Sciences, Fujian Normal University, Fuzhou, China.

²Department of Geography and Planning, University of Toronto, Toronto, ON, Canada. ✉email: janejj.liu@utoronto.ca

insights into the causes of the unexpected ozone increase that occurred during the CLD.

RESULTS AND DISCUSSION

Evidences of stratospheric ozone inputs to surface ozone during the CLD

Normally, the diurnal cycle of surface ozone exhibits a maximum resulting from daytime photochemical reactions and a minimum due to nighttime NO titration. As shown in Fig. 1, before February 14, 2020, the surface ozone concentrations in Beijing increased at a rate of 5–10 ppbv per hour after sunrise, reached a maximum in the afternoon, and then declined thereafter with a minimum in the early morning. However, such a distinct diurnal cycle was absent during February 15–17, 2020 suffering from a deep SI event characterized by high ozone, low CO, and low RH. Taking the average surface ozone during the CLD (23 January–29 February 2020) as a baseline, it is found that ozone concentrations during 15–17 February substantially exceeded the baseline value and persisted over a long period. More impressively, the normal deep valley of nighttime ozone disappeared during 15–17 February, since the nighttime ozone concentrations were significantly enhanced in comparison with those before February 15, 2020. In addition to the abnormally high ozone, surface CO and RH declined synchronously and reached their low valley during 15–17 February. After 18 February, surface ozone returned to its normal diurnal cycle, and CO and RH rebounded significantly. The coevolution of surface ozone, CO, and atmospheric moisture provided pieces of observational evidence for a deep SI event penetrated into the ground level in Beijing during the CLD.

To further confirm the occurrence of this deep SI event, the temporal variations in RH profiles, tropopause height and tropospheric ozone column values are compared in Fig. 2. The average RH profile during 15–17 February was reduced within a deep layer extending from the surface to 300 hPa with reference to that during 10–14 February, and then rebounded vigorously after 18 February (Fig. 2a). Compared with the neighboring periods, low RH values (<30%) dominated in the profiles collected in Beijing during 15–17 February, with a distinct decrease in the atmospheric boundary layer when the stratospheric airmass had penetrated into the ground level. Following the WMO thermal tropopause definition, we find that the tropopause fell down since 13 February and reached a minimum on 15 February. The tropospheric ozone column in Beijing (Fig. 2b), which was

retrieved from MERRA-2 reanalysis data, increased substantially with the falling tropopause height and reached a peak on 15 February, suggesting additional ozone inputs to the troposphere associated with the deep SI event. We further conducted three-dimensional backward trajectory simulations with the HYSPLIT model²⁸ to determine the origin of airmass above Beijing during 15–17 February (Supplementary Fig. 1). The trajectory shows that the airmass initially originated in the stratosphere, descended during the following 8 days to the atmospheric boundary layer height, and then penetrated into the ground level in Beijing within 2 days from the northwest.

The unexpected increase of surface ozone in China during the CLD has drawn a large amount of attention^{1–10}. The causes for this ozone increase have been speculated from the perspectives of chemical responses to the emission reduction and meteorological conditions during the CLD. However, the stratospheric influences on the increase over northern China have not been discussed. Table 1 provides statistics of surface ozone, NO₂, and CO concentrations in Beijing during different periods including the CLD and SI from 1 January to 31 March 2022. Before the lockdown period (pre-CLD, January 1–22, 2020), the average surface ozone in Beijing was 14.84 ppbv, which was enhanced by 9.88 ppbv (66.6%) during the CLD, and increased continuously after the lockdown period (after-CLD, March 1–31, 2020). Similar variations among the three periods were observable for the daytime ozone concentrations, under the influences of photochemical reactions and seasonal evolution of radiation and temperature¹⁵. Due to a 35.7% reduction in NO₂ during the CLD, the titration effect weakened. Therefore, the nighttime ozone increased significantly in Beijing, as reflected in the mean nighttime ozone concentrations. During the deep SI period (February 15–17, 2020), the average daily ozone concentrations reached 32.79 ppbv and exceeded the mean ozone concentrations during the CLD and after-CLD period by 8.07 ppbv and 2.92 ppbv, respectively. We further compared the ozone concentrations in daytime and nighttime separately. For the daytime ozone, the average value during the SI period (33.65 ppbv) exceeded the corresponding value during the CLD (27.96 ppbv). During the night, the ozone difference between the SI and CLD periods was even larger than that during the day. The average nighttime ozone concentrations in Beijing during the SI were ~13 ppbv higher than that during the CLD. As a result, the diurnal variation in surface ozone was dramatically reduced during the SI due to the intrusion of

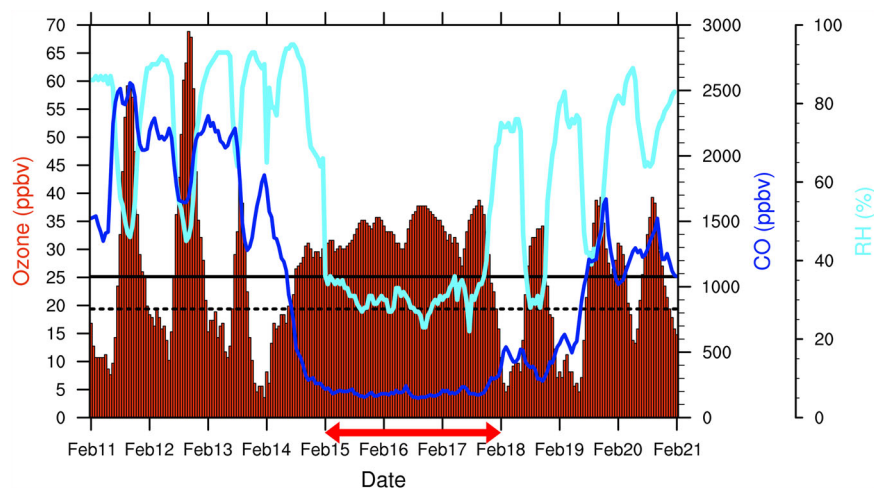


Fig. 1 Evolution of gas pollutants in Beijing. The temporal variations in surface ozone (O₃, red bar), carbon monoxide (CO, blue line) concentrations and relative humidity (RH, cyan line) from 11 to 20 February 2020 during the COVID-19 lockdown (CLD) period in Beijing. The average ozone (horizontal black solid line) and CO (horizontal black dashed line) concentrations during the CLD were used as baseline references. The period when the deep stratospheric intrusion occurred during 15–17 February was marked by the red arrow.

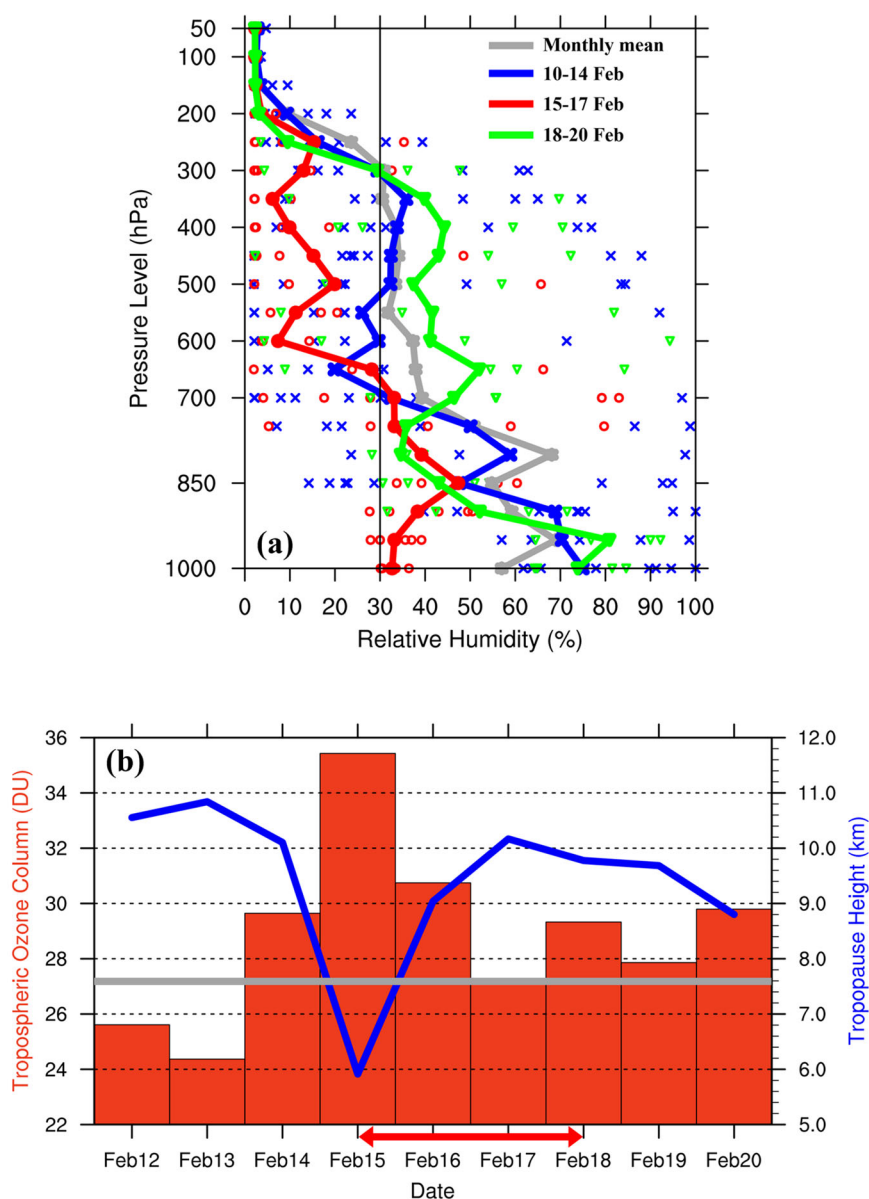


Fig. 2 Evolution of relative humidity (RH) and tropospheric ozone column in Beijing. **a** RH profiles (unit: %) in Beijing averaged over 10–14 February (blue solid line), 15–17 February (red solid line), 18–20 February (green solid line) and 1–29 February (gray solid line, monthly mean values). The scattered cross, circle and triangle symbols represent the RH observations in each selected altitude using the same colors of the corresponding periods. **b** Tropospheric ozone column in Dobson unit (red bar, unit: DU) based on MERRA-2 data and tropopause height (blue line, unit: km) in Beijing based on radiosonde observations. The horizontal gray solid line indicates the monthly mean value of the tropospheric ozone column in Beijing.

Table 1. Statistics of in situ observations of the surface ozone (O_3), NO_2 , CO, SO_2 , and $PM_{2.5}$ concentrations in Beijing during different periods.

Periods	O_3 (ppbv)	O_3 -daytime (ppbv)	O_3 -nighttime (ppbv)	O_3 -range (ppbv)	NO_2 (ppbv)	CO (ppbv)	SO_2 (ppbv)	$PM_{2.5}$ ($\mu g m^{-3}$)
pre-CLD	14.84	16.28	12.40	3.88	23.19	733.59	2.16	41.31
CLD	24.72	27.96	19.30	8.66	14.90	836.27	1.92	72.34
after-CLD	29.87	34.70	21.86	12.84	13.47	453.98	1.48	34.95
SI	32.79	33.65	32.22	1.43	3.68	195.38	0.77	5.90

The statistics include the average O_3 , daytime O_3 (07:00–21:00 local time), nighttime O_3 (22:00–06:00 local time), O_3 range, NO_2 , CO, SO_2 , and $PM_{2.5}$ before (pre-CLD, January 1–22, 2020), during (CLD, 23 January–29 February 2020), after (after-CLD, March 1–31, 2020) the COVID-19 lockdown, and during the deep stratospheric intrusion event (SI, February 15–17, 2020).

stratospheric airmass. The stratospheric influences on other pollutants, i.e., NO_2 , CO , SO_2 , and $\text{PM}_{2.5}$, were also examined. Although vigorous emission reduction was imposed during the CLD, the observed surface NO_2 , CO , SO_2 , and $\text{PM}_{2.5}$ concentrations during the SI were even 2–10 times lower than those during the CLD, indicating a rapid and strong dilution of these pollutants. Compared with the mean concentrations during the CLD, surface NO_2 , CO , SO_2 , and $\text{PM}_{2.5}$ in Beijing during the deep SI event declined by 75.3%, 76.6%, 59.9%, and 91.8%, respectively, reaching the minimum of the entire CLD period. Such overwhelming drops of these pollutants provide additional indications for the deep SI occurrence.

Synoptic conditions of the stratospheric intrusion and responses of ozone over northern China

A cutoff low system characterized by an isolated close circulation formed over northern China and facilitated the SI transport processes (Supplementary Fig. 2). Along with the propagation of the cutoff-low system, airmass with low humidity, high ozone and high potential vorticity (PV) intruded into the middle-to-low troposphere over northern China. Figure 3a shows the horizontal distribution of PV from MERRA-2 data under the influence of the cutoff low system. In addition to the thermal tropopause definition, the 2 PV unit (PVU, $1\text{PVU} = 10^{-6} \text{ m}^2 \text{ s}^{-1} \text{ K kg}^{-1}$) surface is often applied to represent the dynamical tropopause in

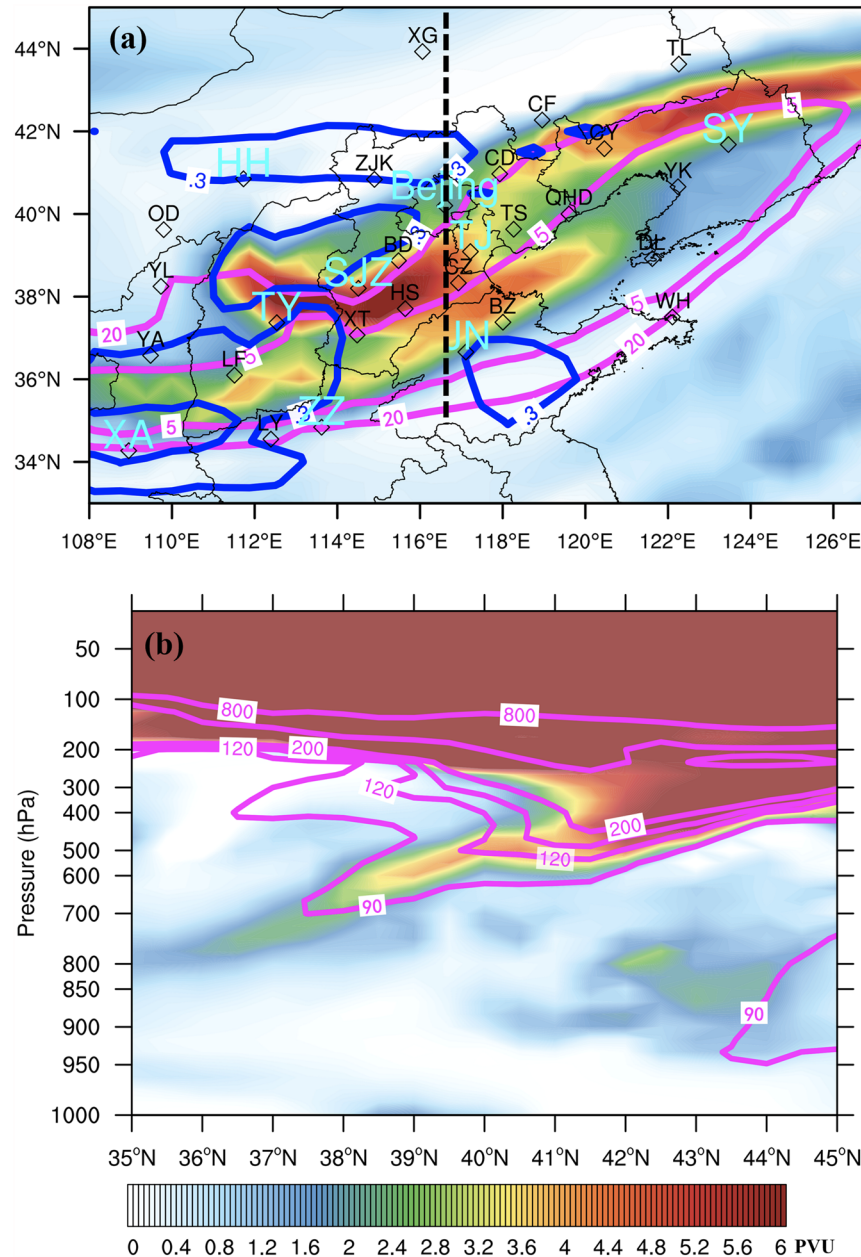


Fig. 3 Distributions of potential vorticity (PV) and ozone over northern China based on MERRA-2 data. **a** Horizontal distribution of PV (color shaded, unit: PVU, $1\text{PVU} = 10^{-6} \text{ m}^2 \text{ s}^{-1} \text{ K kg}^{-1}$) at 500 hPa over northern China at 08:00 local time on February 15, 2020. Dry regions with low RH (5% and 20%) at 850 hPa are marked by magenta lines. Regions with downward air motions ($\omega = 0.3 \text{ pa s}^{-1}$) are marked by blue lines. **b** Vertical cross-section of PV (color shaded) and ozone concentrations (magenta lines, unit: ppbv) along the black dashed line shown in (a). The names of the cities in (a) are abbreviated from their corresponding full names, listed in Table 2.

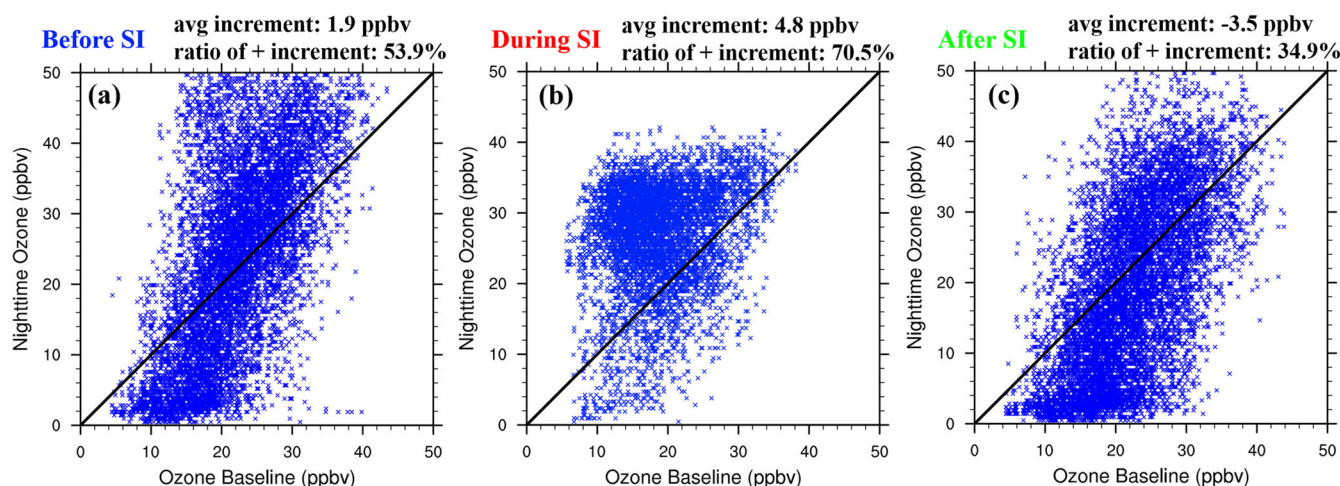


Fig. 4 Variations in nighttime ozone during the SI over northern China. Scatterplot of co-located nighttime (22:00–06:00 local time) surface ozone concentrations (vertical axis) and their corresponding baseline references at the same hours and locations (horizontal axis) before (February 10–14, 2020, **a**), during (February 15–17, 2020, **b**), and after (February 18–20, 2020, **c**) the SI event over northern China. The baseline references are the ozone concentrations before the SI occurrence (23 January–14 February 2020) at the corresponding stations and hours. The average increment of nighttime ozone concentrations relative to their baseline references and the ratio of those with positive increment in each period are indicated above each sub-figure.

synoptic-scale studies^{29,30}. On 15 February 2020, a northeast–southwest-oriented belt with PV exceeding 2 PVU at 500 hPa appeared in most part of northern China, suggesting high-PV airmass had intruded into the middle troposphere. Downward air motions and low moisture were dominated as a result of the SI occurrence. With reference to the cross-section of PV and ozone, a significant deformation of the tropopause (tropopause fold) formed above northern China, where a tongue of air with high PV subsided from the upper troposphere and reached down to 800 hPa. The tropopause fold promoted significant cross-tropopause mass exchange^{31,32}. Along the high-PV tongue, stratospheric ozone-rich airmass was injected into the middle-to-low troposphere. In the north of the PV tongue, high-ozone filament penetrated into the atmospheric boundary layer.

Impacted by the synoptic-scale deep SI following a northwest-to-southeast transport pathway (Supplementary Fig. 1), the diurnal circle of surface ozone over most parts of northern China was interfered alternately (Supplementary Fig. 3). The coexistence of enhanced ozone, declined CO and RH, similar to the corresponding variation patterns in Beijing, was also identifiable in other cities of northern China. Despite the widely distributed stratospheric airmass, however, the magnitudes of surface ozone enhancement during the SI differed from city to city, depending on the distance to the high-PV tongue and the local conditions. Compared with the entire CLD period, the deep SI event inhabited ozone photochemical reactions which was usually seen in the daytime ozone peak before the SI (Fig. 1 and Supplementary Fig. 3), due to the extremely low supply of ozone precursors³³ (such as NO₂ and CO). Still, the injected stratospheric ozone prevailed over the portion of ozone loss in the daytime that was associated with the weakened photochemical reaction, leading to the exceedances of daytime ozone concentrations over their CLD baseline. In view of the fact that the stratospheric air was mixed with the tropospheric air, we examined the nighttime ozone concentrations to avoid the blurring of daytime photochemical reactions, and hence investigated how surface ozone responded to the deep SI over northern China. The stratospheric impacts could be assessed from the difference in ozone concentrations between the SI (15–17 February) and pre-SI (23 January–14 February, within the CLD) periods so that the impacts of other factors could be minimized. Taking the nighttime ozone concentrations over the pre-SI as the baseline references, we show in Fig. 4 the co-located nighttime

ozone concentrations at the same local times. Clearly, the variations in nighttime ozone during the SI event were significantly narrowed, producing an accumulation centering around 25–35 ppbv in comparison with the neighboring periods. On the regional average over all the surface stations distributed over northern China (34–44°N, 108–124°E, the boxed area in Supplementary Fig. 2), the deep SI event led to abnormally high nighttime ozone and enhanced the ozone concentrations from their baseline references by 4.8 ppbv, which even doubled the one before the SI (1.9 ppbv).

Contributions of the stratospheric intrusion to surface ozone increase during the CLD over northern China

The above analyses confirm the occurrence of a deep stratospheric intrusion during the CLD and investigate the responses of surface ozone to the SI event over northern China. Yet, an important question is how much is the injected stratospheric ozone at the surface which had been mixed with local tropospheric ozone. The ratio of stratospheric ozone to the observed surface ozone concentrations provides vital information to understand the impacts of the SI event on surface air quality and ozone variations. In other words, under the CLD scenario with vigorous emission reduction, it is warranted to know to which extent the ozone increase can be explained by the SI event when dealing with the contributions from emission variation and meteorology. Here we estimated the amount of stratospheric ozone (ΔO_3^{strat}) injected during the SI by integrating the excess of ozone concentrations above their baseline references (see “Methods”)^{21,34–36}. Also, the accumulated ozone concentrations during the SI period ($O_3^{SI, sum}$) and during the CLD ($O_3^{CLD, sum}$) were also calculated by integrating the corresponding surface ozone observations. Figure 5a presents the ratios of injected stratospheric ozone to the accumulated ozone concentrations at the surface during the SI period ($100\% \times \frac{\Delta O_3^{strat}}{O_3^{SI, sum}}$). The injected stratospheric ozone largely constituted the surface ozone concentrations during the SI period, even up to 40–45% in some cities, suggesting the dominant role of SI on ozone variations within a short time period. Suffering from this SI event, the mean ozone concentrations during the intrusion days were directly promoted compared with those during the CLD. As noted in ref. ²¹, the contributions of injected stratospheric ozone at the surface are highly sensitive to the period of interest. Even if the injected

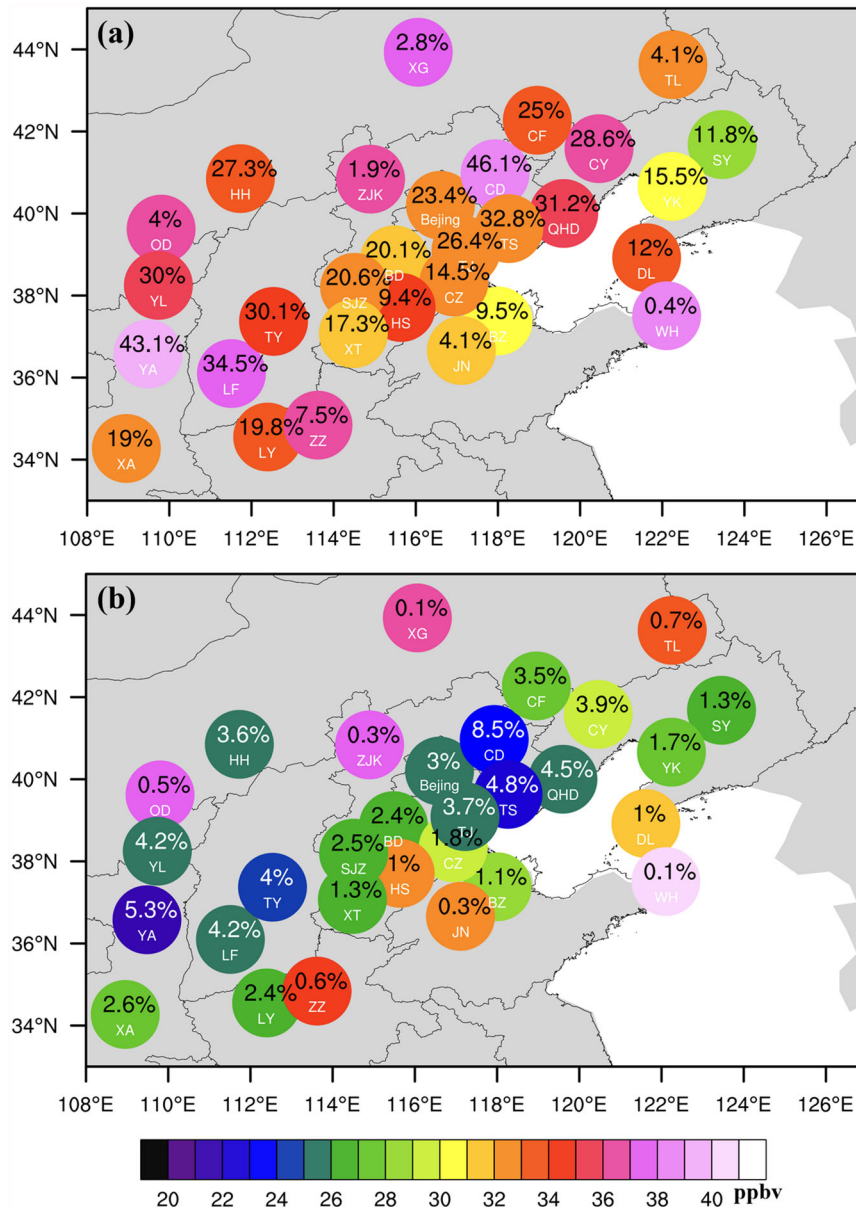


Fig. 5 Mean surface ozone concentrations during the SI and CLD periods. **a** City-scale surface ozone concentrations (unit: ppbv) averaged during the SI period over northern China (color-coded circles placed at the locations of selected cities). The numbers within the color-coded circles indicate the estimated ratios of stratospheric ozone to the accumulated ozone concentration at the surface during the SI period (unit: %, see Eq. (4) in “Methods”). **b** The same as (a), but for the CLD period; the ratios of stratospheric ozone to the accumulated ozone concentrations during the CLD are indicated by the numbers (unit: %, see Eq. (5) in “Methods”). See Table 2 for the abbreviations of the cities’ names.

stratospheric ozone was scaled by the accumulated ozone concentrations during the entire CLD (Fig. 5b; $100\% \times \frac{\Delta O_3^{strat}}{O_3^{CLD}}$), it still accounted for 4–8% of the surface ozone over regions located in the high-PV belt region shown in Fig. 3a.

The unexpected CLD ozone increase relative to that before lockdown¹ reflects the impacts of emission reduction, evolving seasonality of meteorological conditions, and also SI events. Figure 6 shows the amount of injected ozone averaged over the over the entire lockdown period, i.e., the scaled ozone values. In regions associated with high-PV values shown in Fig. 3a, the scaled stratospheric ozone concentrations reached 1–2 ppbv. We calculated the contributions of these additive stratospheric ozone inputs to the overall ozone increase observed during the CLD

(Table 2 and Fig. 6). Though only one SI event occurred, the scaled stratospheric influence contributed 1–18% of the surface ozone increase in different locations during the CLD. Taking Beijing for an example, the ozone increase during the CLD was 9.9 ppbv compared with that before the CLD; this SI event can explain 7.1% of the ozone increase in Beijing during the CLD. Despite different vulnerabilities to the SI processes and different local background ozone concentrations and emission magnitudes, this deep SI event occurred during the CLD and contributed average 5–10% of the overall ozone enhancement over high-PV belt regions (Figs. 3a and 6), suggesting the nonnegligible influences of the SI on ozone variations when disentangling the role of anthropogenic emission controls and meteorological conditions.

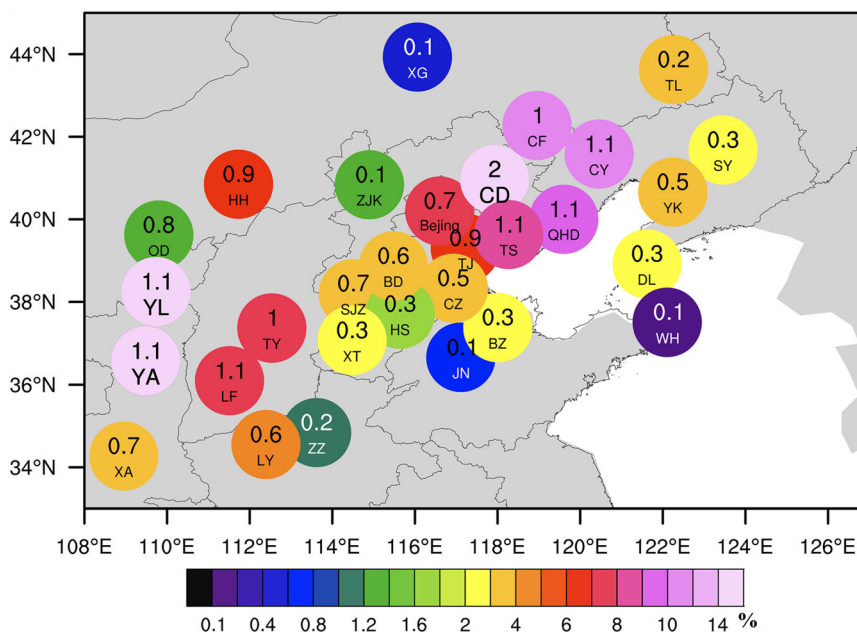


Fig. 6 Stratospheric contributions to the overall ozone enhancement during the CLD over northern China (see Eq. (7) in “Methods”; color-coded circles placed at the locations of selected cities, unit: %). The numbers within color-coded circles indicate the injected stratospheric ozone concentrations scaled over the entire CLD period (i.e., $\frac{\Delta O_3^{strat}}{T_{CLD}}$, T_{CLD} is the time length of the CLD; unit: ppbv). See Table 2 for the abbreviations of the cities’ names.

Lessons from the SI event occurred during the CLD on ozone variations

In previous studies, attempts were made to separate the contributions of vigorous emission reduction and meteorological conditions to the ozone increase during the CLD by comparing between the CLD and the pre-CLD periods. For example, Wang et al.¹⁵ perform numerical simulations with the WRF-Chem model and found that the meteorological factors accounted for 80% of the ozone increase over the Yangtze River Delta (YRD) region of China, while the emission reduction contributed the rest 20%. Li et al.³⁷ attributed 80% of ozone increase during the lockdown period to meteorology over northern China. The CMAQ model results of ref.¹⁴ suggested that the contributions of meteorology and emission reduction to the ozone increase over northern China were 58% and 42%, respectively. However, by means of air quality modeling, Zhao et al.³⁸ believed that meteorology played a relatively minor role, and the precursor emission reduction was the main reason for the observed increase over China during the CLD. Using a machine learning model, Shen et al.¹⁶ argued that meteorology reduced surface ozone by 0.9% in 31 provincial capital cities of China. Viewing the case of central Europe, Cuesta et al.³⁹ estimated that the meteorological conditions accounted for 8% of the overall ozone enhancement during the lockdown, based on a chemistry-transport model simulation. Generally, the ozone inputs from the SI were not explicitly considered in the numerical simulation works mentioned above. As a result, the meteorological contributions to the ozone enhancement relative to emission reduction may be biasedly estimated. This study based on the observational analysis reliably shows that a deep SI event occurred during the lockdown period can contribute an average of 5–10% of the overall ozone enhancement over large parts of northern China. This study suggests that injected stratospheric ozone could impose a nonnegligible impact on ozone pollution during the CLD not only in China but also elsewhere, since the occurrences of deep SIs are not preventable. Therefore, a key lesson is a necessity to take extra account of injected stratospheric ozone in addition to stringent

anthropogenic emission reduction when implementing ozone control strategies in the future.

This study only investigated a SI event with moderate magnitude but long duration during the CLD in China. A higher impact from natural stratospheric ozone inputs on the troposphere would be expected if more deep SI events are identified. Actually, the stratospheric impacts over a specified region depend on the frequency, magnitude and duration of deep SI events as well as the local background ozone. Beyond this SI case occurred during the CLD, it is warranted to examine the characteristics of deep SIs occurring over multiple years, since these understandings aid to offer a more complete insight of natural and anthropogenic influences on surface ozone variations.

METHODS

Air pollutant observations

Hourly ground-based measurements of O_3 , CO, NO_2 , SO_2 , and $PM_{2.5}$ concentrations were obtained from the public website of the Chinese Ministry of Ecology and Environment (MEE) (<https://english.mee.gov.cn/>). The tropospheric ozone column data were retrieved from the Modern-Era Retrospective analysis for Research and Applications version 2 (MERRA-2) reanalysis data. The MERRA-2 is a NASA atmospheric reanalysis using the Goddard Earth Observing System Model, Version 5 (GEOS-5) with its Atmospheric Data Assimilation System (ADAS). The MERRA-2 data have a spatial resolution of 0.5° latitude \times 0.625° longitude with 72 model levels (<https://gmao.gsfc.nasa.gov/reanalysis/MERRA-2/>). We integrated ozone concentrations provided by MERRA-2 from the lowest model level to tropopause height, which is also available in MERRA-2, to obtain the tropospheric ozone column values.

Meteorological data

The surface relative humidity (RH) and operational radiosonde data in Beijing can be downloaded from the National Meteorological Science Data Center (<https://data.cma.cn/>). The MERRA-2 meteorological fields,

Table 2. Top 20 cities with high stratospheric contributions to the overall ozone enhancement during the CLD (last column, see Eq. (7) in “Methods”).

Cities	Ratios of stratospheric ozone during SI (%)	Ratios of stratospheric ozone during CLD (%)	Stratospheric contributions to the overall ozone enhancement during CLD (%)
Chengde (CD)	46.1	8.5	18.9
Yan'an (YA)	43.1	5.3	18.6
Yulin (YL)	30	4.2	14.1
Chaoyang (CY)	28.6	3.9	10.2
Chifeng (CF)	25.0	3.5	10.2
Qinhuangdao (QHD)	31.2	4.5	9.7
Tangshan (TS)	32.8	4.8	8.8
Taiyuan (TY)	30.1	4.0	7.5
Beijing	23.4	3.0	7.1
Linfen (LF)	34.5	4.2	7.1
Tianjin (TJ)	26.4	3.7	6.6
Hohhot (HH)	27.3	3.6	6.0
Luoyang (LY)	19.8	2.4	4.4
Xi'an (XA)	19.0	2.6	3.8
Shijiazhuang (SJZ)	20.6	2.5	3.6
Yingkou (YK)	15.5	1.7	3.6
Baoding (BD)	20.1	2.4	3.4
Cangzhou (CZ)	14.5	1.8	3.0
Tongliao (TL)	4.1	0.7	3.0
Dalian (DL)	12.0	1.0	2.7

The ratios of stratospheric ozone during the SI and CLD periods in these cities are also shown.

including PV, geopotential height, temperature, horizontal winds, RH, and vertical velocity, were used in this study.

Backward trajectory simulations

The National Oceanic Atmospheric Administration’s (NOAA) hybrid single-particle Lagrangian integrated trajectories (HYSPPLIT) model is widely used in studies of air pollutant transport (<https://www.arl.noaa.gov/hysplit>). We applied the HYSPLIT model to identify the origins and pathways of air mass reaching Beijing during the SI period. The back trajectories were simulated using the Global Forecast System (GFS) 0.25° meteorological dataset.

Estimation of the impacts of the stratospheric intrusion on surface ozone

The mean surface ozone concentrations at each hour were calculated by averaging ozone observations at each of the 24 h covering two different periods. The first set of hourly means is for the period of the CLD before SI (23 January–14 February 2020, namely $\overline{O_{3h}^{P1}}$, where $h = 1-24$), and the second set is for the pre-CLD within the CLD period (January 1–22, 2020, namely $\overline{O_{3h}^{P2}}$, where $h = 1-24$). These two sets of hourly mean values provide baseline references to quantitatively separate the influences of the stratospheric intrusion, emission reduction and meteorology during the CLD. In other words, the difference in ozone concentrations during the SI and $\overline{O_{3h}^{P1}}$ could be attributed to the

stratospheric intrusion, while the difference in ozone concentrations during the CLD and $\overline{O_{3h}^{P2}}$ could be attributed to the stratospheric intrusion, emission reduction and meteorology. This methodology was inspired by previous studies^{21,34–36} with some modifications. Specifically, the excess of ozone above the baseline references during the SI period was integrated (Eq. (1)), which was taken as the amount of injected stratospheric ozone (ΔO_3^{strat}).

$$\Delta O_3^{strat} = \int_{SI_start}^{SI_end} \int_{h_start}^{h_end} (O_{3h,t} - \overline{O_{3h}^{P1}}) dh dt \quad (1)$$

where $O_{3h,t}$ denotes the ozone observations at hour h and day t , and the $\overline{O_{3h}^{P1}}$ represents the ozone reference concentrations at the same hour. The differences between $O_{3h,t}$ and $\overline{O_{3h}^{P1}}$ were summed over the period of SI occurrence with a temporal resolution of 1 h. Generally, $h_start = 1$ and $h_end = 24$, except for the start and end days of SI when the actual hours were used.

The sum of ozone concentrations during the SI and CLD periods were calculated following Eqs. (2) and (3), respectively.

$$O_{3SI}^{sum} = \int_{SI_start}^{SI_end} \int_{h_start}^{h_end} O_{3h,t} dh dt \quad (2)$$

$$O_{3CLD}^{sum} = \int_{CLD_start}^{CLD_end} \int_{h_start}^{h_end} O_{3h,t} dh dt \quad (3)$$

The ratios of stratospheric ozone to the sum of ozone concentrations during the SI and CLD period were given by

$$Ratio_{SI} = 100\% * \frac{\Delta O_3^{strat}}{O_{3SI}^{sum}} \quad (4)$$

$$Ratio_{CLD} = 100\% * \frac{\Delta O_3^{strat}}{O_{3CLD}^{sum}} \quad (5)$$

The ozone enhancement during the CLD (ΔO_3) relative to that before the lockdown (pre-CLD) period contains the impacts of emission reduction, meteorology and stratospheric intrusions. Provided with the additive stratospheric ozone, the stratospheric contributions to the overall ozone enhancement during the CLD were calculated following

$$\Delta O_3 = \int_{CLD_start}^{CLD_end} \int_{h_start}^{h_end} (O_{3h,t} - \overline{O_{3h}^{P2}}) dh dt \quad (6)$$

$$Contribution^{strat} = 100\% * \frac{\Delta O_3^{strat}}{\Delta O_3} \quad (7)$$

DATA AVAILABILITY

Datasets are freely available and can be downloadable from the internet and are available upon request.

CODE AVAILABILITY

The codes used in this study are available upon request.

Received: 19 March 2023; Accepted: 19 June 2023;

Published online: 29 June 2023

REFERENCES

- Le, T. et al. Unexpected air pollution with marked emission reductions during the COVID-19 outbreak in China. *Science* **369**, 702–706 (2020).
- Shi, X. & Brasseur, G. P. The response in air quality to the reduction of Chinese economic activities during the COVID-19 outbreak. *Geophys. Res. Lett.* **47**, e2020GL088070 (2020).

3. Silver, B., He, X. Y., Arnold, S. R. & Spracklen, D. V. The impact of COVID-19 control measures on air quality in China. *Environ. Res. Lett.* **15**, 084021 (2020).
4. Li, M. et al. Drivers for the poor air quality conditions in North China Plain during the COVID-19 outbreak. *Atmos. Environ.* **246**, 118103 (2021).
5. Huang, X. et al. Enhanced secondary pollution offset reduction of primary emissions during COVID-19 lockdown in China. *Natl Sci. Rev.* **8**, nwa137 (2021).
6. Zhu, S. et al. Comprehensive insights into O₃ changes during the COVID-19 from O₃ formation regime and atmospheric oxidation capacity. *Geophys. Res. Lett.* **48**, e2021GL093668 (2021).
7. Su, T., Li, Z., Zheng, Y., Luan, Q. & Guo, J. Abnormally shallow boundary layer associated with severe air pollution during the COVID-19 lockdown in China. *Geophys. Res. Lett.* **47**, e2020GL090041 (2020).
8. Zhu, J. et al. Enhanced PM_{2.5} decreases and O₃ increases in China during COVID-19 lockdown by aerosol-radiation feedback. *Geophys. Res. Lett.* **48**, e2020GL090260 (2021).
9. Shi, Z. et al. Abrupt but smaller than expected changes in surface air quality attributable to COVID-19 lockdowns. *Sci. Adv.* **7**, eabd6696 (2021).
10. Kroll, J. H. et al. The complex chemical effects of COVID-19 shutdowns on air quality. *Nat. Chem.* **12**, 777–779 (2020).
11. Fu, X. et al. Persistent heavy winter nitrate pollution driven by increased photochemical oxidants in northern China. *Environ. Sci. Technol.* **54**, 3881–3889 (2020).
12. Leung, D. et al. Wintertime particulate matter decrease buffered by unfavorable chemical processes despite emissions reductions in China. *Geophys. Res. Lett.* **47**, e2020GL087721 (2020).
13. He, J. et al. Multi-year application of WRF-CAMS over East Asia-Part I: comprehensive evaluation and formation regimes of O₃ and PM_{2.5}. *Atmos. Environ.* **165**, 122–142 (2017).
14. Liu, Y. et al. Diverse response of surface ozone to COVID-19 lockdown in China. *Sci. Total Environ.* **789**, 147739 (2021).
15. Wang, H. et al. Seasonality and reduced nitric oxide titration dominated ozone increase during COVID-19 lockdown in eastern China. *npj Clim. Atmos. Sci.* **5**, <https://doi.org/10.1038/s41612-022-00249-3> (2022).
16. Shen, F. et al. Disentangling drivers of air pollutant and health risk changes during the COVID-19 lockdown in China. *NPJ Clim. Atmos. Sci.* **5**, <https://doi.org/10.1038/s41612-022-00276-0> (2022).
17. Stohl, A. et al. Stratosphere-troposphere exchange—a review, and what we have learned from STACCATO. *J. Geophys. Res.* **108**, 8516 (2003).
18. Langford, A. O., Aikin, K. C., Eubank, C. S. & Williams, E. J. Stratospheric contribution to high surface ozone in Colorado during springtime. *Geophys. Res. Lett.* **36**, L12801 (2009).
19. Trickl, T. et al. Forecasted deep stratospheric intrusions over Central Europe: case studies and climatologies. *Atmos. Chem. Phys.* **10**, 499–524 (2010).
20. Kuang, S. et al. Stratosphere-to-troposphere transport revealed by ground-based lidar and ozonesonde at a midlatitude site. *J. Geophys. Res.* **117**, D18305 (2012).
21. Elbern, H., Kowol, J., Sladkovic, R. & Ebel, A. Deep stratospheric intrusions: a statistical assessment with model guided analyses. *Atmos. Environ.* **31**, 3207–3226 (1997).
22. Lawrence, M. G., Kuhlmann, R., Salzmann, M. & Rasch, P. J. The balance of effects of deep convective mixing on tropospheric ozone. *Geophys. Res. Lett.* **30**, 18 (2003).
23. Chen, Z. et al. Transport of substantial stratospheric ozone to the surface by a dying typhoon and shallow convection. *Atmos. Chem. Phys.* **22**, 8221–8240 (2022).
24. Dreessen, J. A sea level stratospheric ozone intrusion event induced within a thunderstorm gust front. *B. Am. Meteorol. Soc.* **100**, 1259–1275 (2019).
25. Davies, T. & Schuepbach, E. Episodes of high ozone concentrations at the earth's surface resulting from transport down from the upper troposphere/lower stratosphere: a review and case studies. *Atmos. Environ.* **28**, 53–68 (1994).
26. Lal, S. & Lawrence, M. G. Elevated mixing ratios of surface ozone over the Arabian Sea. *Geophys. Res. Lett.* **28**, 1487–1490 (2001).
27. Wang, H., Wang, W., Huang, X. & Ding, A. Impacts of stratosphere-to-troposphere transport on summertime surface ozone over eastern China. *Sci. Bull.* **65**, 276–279 (2020).
28. Stein, A. F. et al. NOAA's HYSPLIT atmospheric transport and dispersion modeling system. *B. Am. Meteorol. Soc.* **96**, 2059–2077 (2015).
29. Kunz, A., Konopka, P., Müller, R. & Pan, L. L. Dynamical tropopause based on isentropic potential vorticity gradients. *J. Geophys. Res.* **116**, D01110 (2011).
30. Li, D., Bian, J. C. & Fan, Q. J. A deep stratospheric intrusion associated with an intense cut-off low event over East Asia. *Sci. China Earth Sci.* **58**, 116–128 (2015).
31. Li, D. & Bian, J. C. Observation of a summer tropopause fold by ozonesonde at Changchun, China: comparison with reanalysis and model simulation. *Adv. Atmos. Sci.* **32**, 1354–1364 (2015).
32. Song, Y. et al. The impact of cut-off lows on ozone in the upper troposphere and lower stratosphere over Changchun from ozonesonde observations. *Adv. Atmos. Sci.* **33**, 135–150 (2016).
33. Bradshaw, J. et al. Observed distributions of nitrogen oxides in the remote free troposphere from the NASA global tropospheric experiment programs. *Rev. Geophys.* **38**, 61–116 (2000).
34. Cristofanelli, P. et al. A 6-year analysis of stratospheric intrusions and their influence on ozone at Mt. Cimone (2165 m above sea level). *J. Geophys. Res.* *Atmos.* **111**, D03306 (2006).
35. Cristofanelli, P. et al. Tropospheric ozone variations at the Nepal Climate Observatory-Pyramid (Himalayas, 5079 m a.s.l.) and influence of deep stratospheric intrusion events. *Atmos. Chem. Phys.* **10**, 6537–6549 (2010).
36. Lin, Y.-C. et al. Stratospheric influence on the concentration and seasonal cycle of lower tropospheric ozone: observation at Mount Hehuan, Taiwan. *J. Geophys. Res.* *Atmos.* **119**, 3527–3536 (2014).
37. Li, R. et al. Substantial changes in gaseous pollutants and chemical compositions in fine particles in the North China Plain during the COVID-19 lockdown period: anthropogenic vs. meteorological influences. *Atmos. Chem. Phys.* **21**, 8677–8692 (2021).
38. Zhao, Y. B. et al. Substantial changes in nitrogen dioxide and ozone after excluding meteorological impacts during the COVID-19 outbreak in mainland China. *Environ. Sci. Technol. Lett.* **7**, 402–408 (2020).
39. Cuesta, J. et al. Ozone pollution during the COVID-19 lockdown in the spring of 2020 over Europe, analysed from satellite observations, in situ measurements, and models. *Atmos. Chem. Phys.* **22**, 4471–4489 (2022).

ACKNOWLEDGEMENTS

This work was supported by the National Natural Science Foundation of China (Grant No. 42105079). The computing resources used in this study were provided by Fujian Normal University High-Performance Computation Center (FNU-HPCC). We thank Lingyun Meng from Nanjing University for her help with data processing. We appreciate the efforts from the Chinese Ministry of Ecology and Environment for supporting the nationwide observation network and publishing hourly air pollutant concentrations. We also thank NASA GMAO for the MERRA-2 reanalysis data and NOAA for the HYSPLIT model.

AUTHOR CONTRIBUTIONS

Conceptualization: Z.C. and J.L. Methodology: Z.C. and J.L. Investigation: Z.C., J.L., X.C., M.Y., and L.S. Visualization: Z.C. and J.L. Supervision: J.L. Writing—original draft: Z.C. Writing—review and editing: Z.C., J.L., X.C., M.Y., and L.S.

COMPETING INTERESTS

The authors declare no competing interests.

ADDITIONAL INFORMATION

Supplementary information The online version contains supplementary material available at <https://doi.org/10.1038/s41612-023-00406-2>.

Correspondence and requests for materials should be addressed to Jane Liu.

Reprints and permission information is available at <http://www.nature.com/reprints>

Publisher's note Springer Nature remains neutral with regard to jurisdictional claims in published maps and institutional affiliations.



Open Access This article is licensed under a Creative Commons Attribution 4.0 International License, which permits use, sharing, adaptation, distribution and reproduction in any medium or format, as long as you give appropriate credit to the original author(s) and the source, provide a link to the Creative Commons license, and indicate if changes were made. The images or other third party material in this article are included in the article's Creative Commons license, unless indicated otherwise in a credit line to the material. If material is not included in the article's Creative Commons license and your intended use is not permitted by statutory regulation or exceeds the permitted use, you will need to obtain permission directly from the copyright holder. To view a copy of this license, visit <http://creativecommons.org/licenses/by/4.0/>.